Paper CIT02-0863

BLUFF-BODIES VORTEX SHEDDING SUPRESSION BY DIRECT NUMERICAL SIMULATION

Paulo Augusto Rodrigues Ribeiro
Instituto de Pesquisas Hidráulicas, Universidade Federal do Rio Grande do Sul – Av. Bento Gonçalves, 9500 – 91501-970
Porto Alegre – RS – Brazil
parribeiro@yahoo.com

Edith Beatriz Camaño Schettini
Instituto de Pesquisas Hidráulicas, Universidade Federal do Rio Grande do Sul – Av. Bento Gonçalves, 9500 – 91501-970
Porto Alegre – RS – Brazil
bcamano@iph.ufrgs.br

Jorge Hugo Silvestrini
Departamento de Engenharia Mecânica e Mecatrônica, Pontifícia Universidade Católica do Rio Grande do Sul – Av Ipiranga, 6681
– 90619-900 – Porto Alegre – RS – Brazil
jorgehs@em.pucrs.br

Abstract. Vortex shedding is responsible for harmful vibrations on immersed structures and for increasing their drag coefficients. Thus vortex shedding suppression is highly interesting in order of decrease maintenance costs of standing structures and fuel costs on moving ones. Vortex shedding suppression is here achieved with the use of splitter plates by means of numerical simulations at a low Reynolds range, Re 100 and 160. For this purpose it has been used a high order finite difference method in association with a virtual boundary method, responsible for the obstacle's representation. The use of this novel numerical method showed a great concordance with experimental results by means of low computational costs.

Keywords. vortex shedding, turbulence, numerical simulation, virtual boundary method

1. Introduction

Vortex shedding from circular cylinders have always been a subject of interest, both for experimentalists and for numerical researchers, thanks to its geometrical simplicity in addition to its practical importance in engineering. Nevertheless the flow at low Reynolds numbers has recently achieved great attention due to the advances on the understanding of three-dimensional developments on circular cylinder wakes, after studies carried out by Williamson (1989) on the discontinuity on the Strouhal-Reynolds curve around $Re = 70$, and Williamson (1996) on the recognition of vortex shedding Mode-A and Mode-B for wake transient régimes.

Since then, the spotlights have focus on the understanding of flow instability phenomena and on its control of vortex shedding. A fine summary of vortex shedding control techniques is carried out by Schumm et al. (1994), the authors present two families of vortex shedding control techniques: the open-loop control techniques, i.e. those who introduce physical changes on the obstacle, such as the use of geometrical disturbances, splitter plates, wall rotation among others; and the close-loop control techniques that consist of changing the flow characteristics just like base bleed, base suction, wake heating, control wire, feed-back control, etc.

Among this techniques the use of splitter plates is surely one of the first approaches studied, Roshko (1954) presents experiments using splitter plates where he shows that vortex shedding can be completely suppressed at $Re = 1.45 \cdot 10^4$ for a plate length (l) equal to $5D$, where D is the cylinder's diameter. Bearman (1965) showed that the vortex shedding suppression for square cylinders with splitter plates at Reynolds numbers between $1.4 \cdot 10^5$ and $2.56 \cdot 10^6$ occurs, for all cases studied, for $l/D = 3$.

There are few numerical simulations concerning the transient wake régime, $100 < Re < 300$, for example one can quote Know and Choi (1996) who studied vortex shedding suppression with splitter plates for Reynolds numbers between $80 < Re < 160$, avoiding this way the three-dimensionality that occurs for Reynolds numbers higher than 160. In this paper numerical simulations were performed at $Re = 100$ and $Re = 160$ finding a great agreement with the previous authors results. There are presented as well some results at $Re = 300$ where one finds some puzzling features on the interaction between the plate's boundary layer and the wake structures.

2. Numerical Methods

Uncompressible flows were simulated using the governing equations

$$\vec{\nabla} \cdot \vec{u} = \boldsymbol{0} \, , \tag{1}$$

$$\frac{\partial \vec{u}}{\partial t} + \vec{u} \cdot \vec{\nabla} \vec{u} = -\frac{\boldsymbol{1}}{\boldsymbol{r}} \vec{\nabla} p + \boldsymbol{n} \nabla^2 \vec{u} + \vec{f} \, . \tag{2}$$

On these equations one has $\boldsymbol{n}$ as kinematic viscosity, $p(\vec{x}, t)$ the pressure field, $\vec{u}(\vec{x}, t)$ the velocity field and $\vec{f}(\vec{x}, t)$ the external forcing field, used to represent the virtual boundary.

This external forcing field, introduced by Goldstein et al. (1993), can be described as a harmonic oscillator like

$$\vec{f}(x_s, t) = \boldsymbol{a} \int_0^t \vec{u}(x_s, t) dt + \boldsymbol{b} \, \vec{u}(x_s, t). \tag{3}$$

The time integration has been done using a low-storage third-order Runge-Kutta scheme introduced by Williamson (1980), and spatial derivates were calculated using a sixth-order compact finite difference scheme presented by Lele (1992) over a cartesian uniform grid. Boundary conditions were set to be semi-periodic on y and non-periodic on x, as presented at Fig. (1). More details about the numerical code and the immersed boundary methods used can be found in Silvestrini and Lamballais (2002) and Lamballais and Silvestrini (2002).
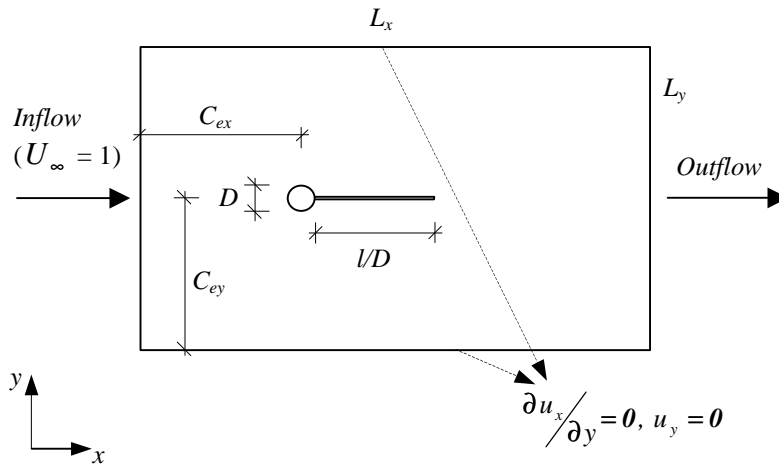

Figure 1. Flow configuration.

3. Computational Domain

It was performed several test simulations at $Re = 300$ to define the necessary computational domain. These simulations aimed to analyze optimal L_x, L_y, C_{ex}, C_{ey}, $\boldsymbol{a}$ and $\boldsymbol{b}$ values in order to minimize computational costs.

First parameters to be analysed, the uniform mesh domain sizes L_x and L_y were defined taking into account a minimum entrance distance, C_{ex} and C_{ey}, equal to $6D$. Different C_{ex} values, $6D$, $8D$ and $10D$ were tested, in all cases for simulations the use of a numerical filtering (Silvestrini and Lamballais, 2002) showed to be essential in order to minimize mean signal oscillations, as shown in Fig. (2a).

However, as suggested by Fig (2b), the effect of the minimum entrance distance's on the flow pattern showed to be negligible by the presented mean flow profiles and by their Strouhal Number values, who showed a maximum 1.5% difference, $S_{6D} = 0.194$, $S_{8D} = 0.192$ and $S_{10D} = 0.191$.

The domain extension L_x were defined by qualitative observation of the vortex street dissipation behind the obstacle, and it has been this way defined a minimum L_x extension equal to $19D$, where there were left $13D$ for the vortex translation concerning the minimum $6D$ entrance distance.

In order to study L_y domain size's confinement influence, there were performed simulations with different L_y dimensions, just like $12D$, $16D$, $24D$ and $32D$. Figure (3) shows mean longitudinal U_x velocity profiles for different L_y at $y/D = 0$, i.e. at the cylinders center, one can see that as the domain size L_y increases the mean velocity U_x at the lateral limits tends to the flow external velocity, U , equal to 1, although it does not get to it.

Mean longitudinal U_x velocity at the L_y limits are $U_{x12D} = 1.040$, $U_{x16D} = 1.017$, $U_{x24D} = 1.004$ and $U_{x32D} = 1.001$, and their respective Strouhal Numbers are $S_{12D} = 0.194$, $S_{16D} = 0.194$, $S_{24D} = 0.193$ and $S_{32D} = 0.193$. From this values one can note that changing L_y from $12D$ to $32D$, despite the mean U_x velocity decreasing 3.8%, the wake's shedding frequency changes nearly 0.6% suggesting that the $L_y = 12D$ transversal domain size has a small influence on the wake shedding pattern.
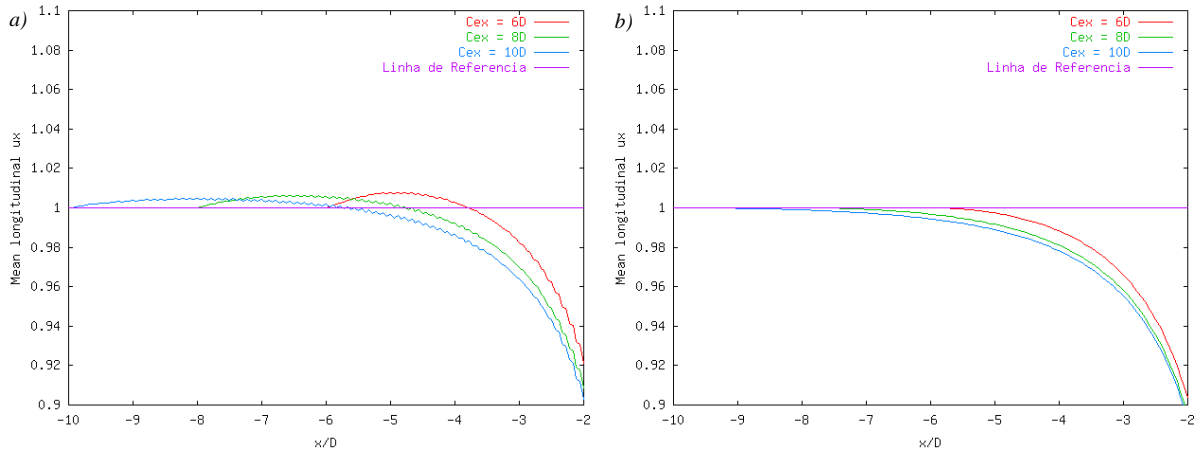
Figure 2. Mean longitudinal U_x velocity profiles at $y/D = 0$: *a)* without filtering and *b)* with filtering.

One intriguing question concerning the virtual boundary method is whether its **a** and **b** coefficients affect or not the wake's shedding frequency. While **b** dampens the oscillation of the forcing field response, the coefficient **a** is related to its response frequency, and, as cited by Saiki and Biringen (1996) it might produce this response with a natural frequency higher than highest frequencies presented in the flow so the force field can respond correctly to the changing flow field. In order to check these parameters influence on the wake's patterns there were performed several simulations with different **a** and **b** combinations: **a** = -40000, **b** = -60; **a** = -10000, **b** = -150; **a** = -4000, **b** = -60; **a** = -4000, **b** = -6.
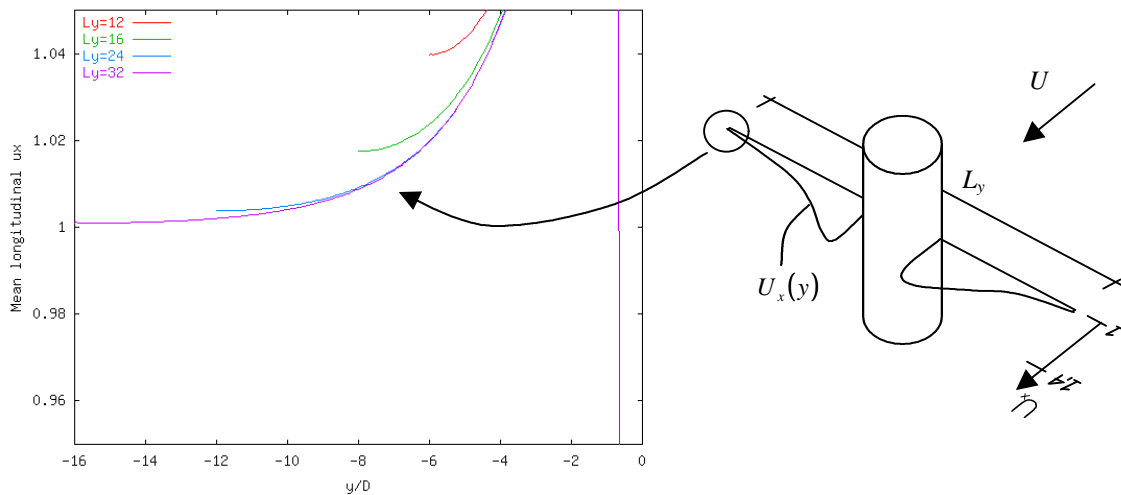

Figure 3. Mean longitudinal U_x velocity profiles at $x/D = 0$.

As expected the obstacle's representation gets better as the **a** and **b** parameters pair has increasing values, which means that the forcing field is "informed" to the flow with a higher frequency thus resulting in lower velocities over the obstacles boundary points, as suggested by the Fig. (4) where one can find L^2 *norm* values defined by

$$L^2 \; norm = \|u\|_2 = \left(\int_{-\infty}^{\infty} |u(x)|^2 \, dx \right)^{1/2}. \tag{4}$$

Although one can notice that the L^2 *norm* in the logarithmical representation of Fig. (4), it may be said that the decreasing oscillation's average does not affect the wake's development at all, as it can be seen by their respective Strouhal Number: $S_{a=-40000; \; b=-60} = 0.193$; $S_{a=-10000; \; b=-60} = 0.195$; $S_{a=-4000; \; b=-60} = 0.195$; $S_{a=-4000; \; b=-6} = 0.194$, where one can notice a maximum difference of barely 0.6%.

The choice of the **a** and **b** coefficient pair is important once the time step of the simulation depends on it. In this work, were chosen **a** = -4000 and **b** = -6 because it results in no penalties for the time step.

The simulation's parameter that most affects the wake is, no doubt, the mesh refinement. Defining the number of grid points per diameter is a crucial input to the simulations performance. However once one works with uniform grid, the refinement is very costly and the search of a cost-effective number of points is a key factor on this numerical simulation method.
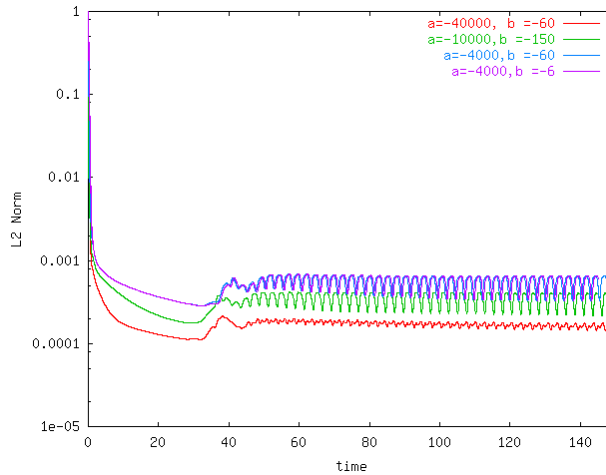
3

Figure 4. L^2 *norm* at the obstacle's virtual boundary vs. computational time.

Simulations with different mesh refinement were carried out with $D = 12\textbf{D}$, $D = 18\textbf{D}$, $D = 24\textbf{D}$ and $D = 32\textbf{D}$, where **D** is the size of the mesh grid. In the first instance, the $D = 12\textbf{D}$ resolution showed itself incapable of representing the flow field at some Reynolds number, being this way discarded. Table (1) provides a comparison between Strouhal numbers for different Reynolds numbers and on different mesh resolutions.

Table 1. Strouhal number values for different Reynolds numbers and mesh resolutions.

Re	Experimental (Williamson, 1989)	$D = 18\textbf{D} - 2D$	$D = 24\textbf{D} - 2D$	$D = 32\textbf{D} - 2D$
100	0.164	0.162	0.166	0.169
200	0.184	0.185	0.191	-
300	0.203	0.194	0.202	0.205

Figure (5) shows a comparison between experimental results by Williamson (1989) and numerical results. One can notice the small divergence between the experimental result at $Re = 100$ and the one observed with the best mesh resolution $D = 32\textbf{D}$, that would be expected to be nearly the same. Despite the disagreement between the expected best numerical result and the experimental one, this 2.8% difference agrees perfectly with other experimental results like those obtained by Roshko (1954), $S = 0.167$, and those by Berger and Wille (1972), $S = 0.16\text{-}0.17$. This allows to conclude that the great achievement of mesh resolution $D = 18\textbf{D}$ may be not due its best performance to simulate the flow at this Reynolds number.
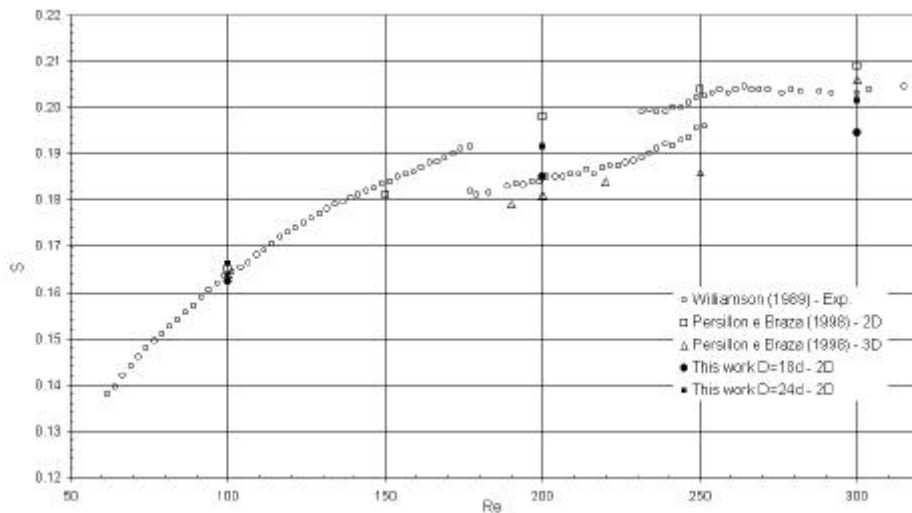

Figure 5. Strouhal number vs. Reynolds number; experimental and numerical results.

This happens once again at $Re = 200$, where there is the transitional wake phenomena, because the experimental value could never be reached by a bi-dimensional numerical simulation once it is due to a three-dimensional phenomena on the flow known as Mode-A transition, as shown by Pérsillon and Braza (1998), who obtained $S = 0.198$ on a 2D simulation and 0.181 on a 3D simulation. In this way, the higher Strouhal number value obtained on the $D = 24\boldsymbol{D}$ simulation confirms that this suspicious good agreement achieved by the $D = 18\boldsymbol{D}$ simulation is once more associated with result corruption.

At $Re = 300$, where there is a completely turbulent wake, it can be clearly seen that the best results are obtained with the finer mesh which have good agreement with experimental results. The mesh $D = 18\boldsymbol{D}$ results in a Strouhal number 4.2% smaller in comparison with experimental results, once again one can notice the corrupting effect of this mesh coarseness. However it is worth make it clear that although one obtains poor results in comparison with a finer mesh, this resolution is frequently the preferred one once it implies in a much smaller computational cost, specially for providing greater possibilities in three-dimensional calculations. In the following simulations it has been used $D = 24\boldsymbol{D}$.

Another interesting characteristic of the coarse mesh is the amplification of the flow oscillation in front of the obstacle, as shown in Fig. (6). It is not understood yet whether this oscillations are harmful or not to the wake.
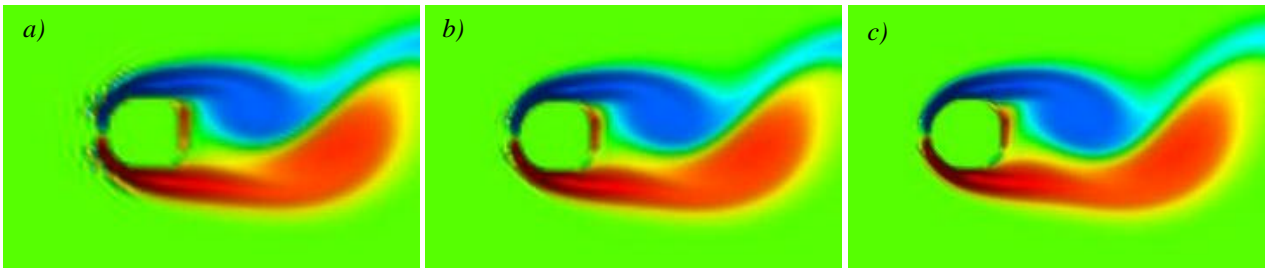

Figure 6. Zoom on the cylinder's proximity for $Re = 100$: *a)* $D = 18\boldsymbol{D}$, *b)* $D = 24\boldsymbol{D}$ and *c)* $D = 32\boldsymbol{D}$.

4. Flow around cylinders with splitter plates

4.1. Two-dimensional flows

It is known that vortex shedding may be suppressed by the introduction of splitter plates on the wake of bluff-bodies. Roshko (1993), per example, affirms that depending on cylinder cross-section shape, a plate length of 7 to 10 diameters is sufficiently long for the near wake to be independent of that length. Usually this phenomena is used as a model to analyze the role of the separated shear layers and drag, like in the works of Arie and Rouse (1956), Roshko (1954) and Roshko (1993).

Perhaps, one of the first attempt to understand the role of three-dimensionality on the shedding of bluff-bodies with attached plates is introduced by Bearman (1965), who described régimes on the variation of Strouhal number on different plate lengths for a square cylinders at Reynolds numbers between $1.4 \cdot 10^{5}$ and $2.56 \cdot 10^{6}$, in all cases he found vortex shedding suppression for $l/D = 3$.

On a numerical attempt of finding this same phenomena, Know and Choi (1996) studied vortex shedding suppression for the two-dimensional wake régime, $80 \le Re \le 160$, and these authors found great agreement with Bearman's results.

The present simulations at $Re = 100$ showed great agreement with those obtained by Know and Choi (1996), vortex shedding has been suppressed for a plate length equal to $l/D = 3$, and for l/D equal to 1 and 2 values differ 3.6% and 7.5% respectively, as can be seen at Fig. (7).
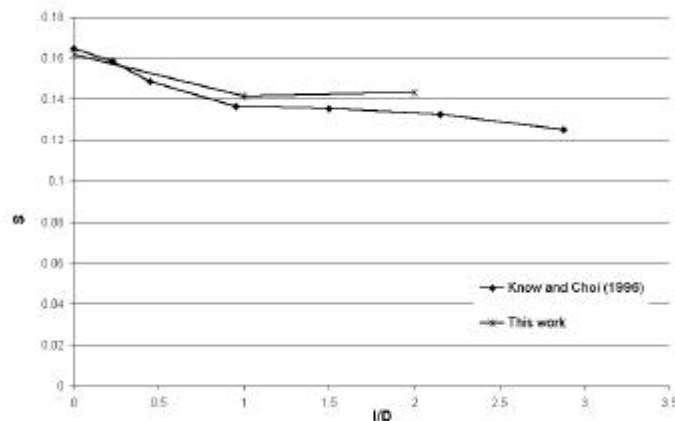
Figure 7. Strouhal number vs. plate length behind circular cylinder at $Re = 100$.

Those differences may be interpreted as influence of an extensively greater domain by the first authors, $-50D < x < 20D$ and $-50D < y < 50D$, and the use of a finer mesh near the cylinder. Nevertheless it is very important to emphasize that these simulations that solve the Navier Stokes over a curvilinear mesh consumes enormous time and computational resources compared by those performed in this work over a uniform cartesian mesh, which also achieve great results, being possible better used based on a cost effectivity criteria.

In Fig. (8) one can see qualitatively the wake's behavior due the plate's presence. The clearly represented vortex street of Fig. (8a) suffers a strong reduction on its shedding frequency when there is the plate's introduction, Fig. (8b) and Fig. (8c), until the flow reattaches to the plate and vortex shedding is simply suppressed.
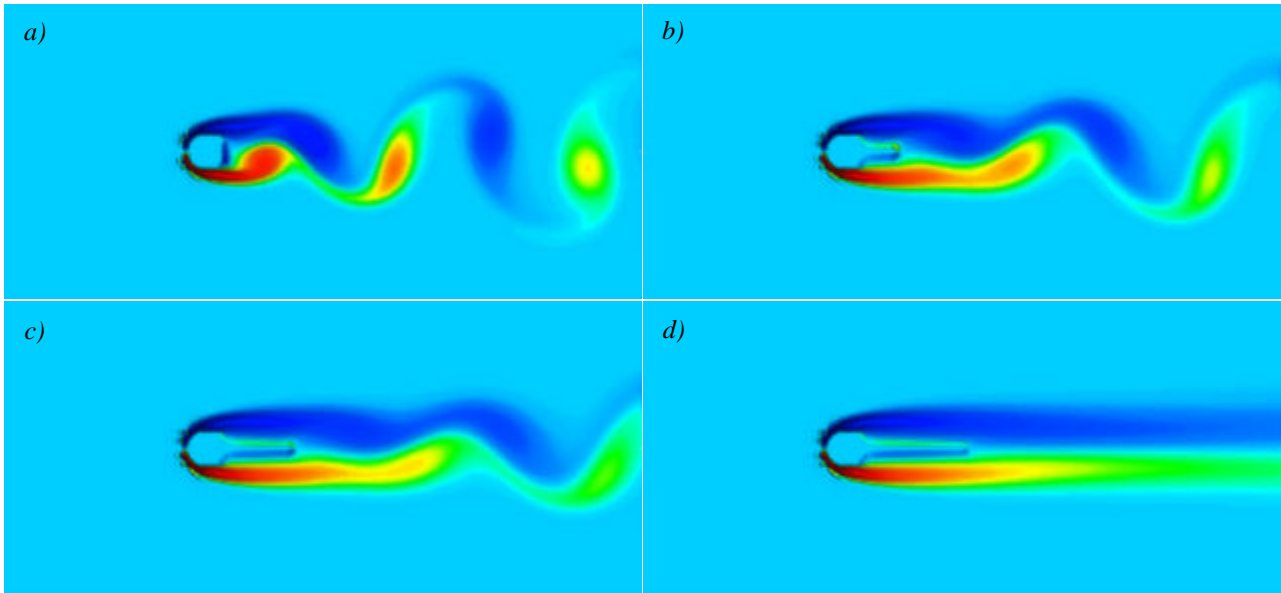

Figure 8. Vorticity field for $Re = 100$ at time $t \cdot U_\infty/D = 347$; a) no plate, b) l/D = 1, c) l/D = 2 and d) l/D = 3.

At $Re = 160$ it had as well been observed that the vortex shedding was indeed suppressed in comparison with Know and Choi's results. At Fig. (9a) one can see the vortex street pattern for a plate length $l/D = 4$ and the flow filed with suppressed vortex shedding for a plate length $l/D = 5$. This results have great agreement with Know and Choi (1996) because besides the Strouhal number for $l/D = 4$ which differs just 3.3%, the authors point the critical plate length $l/D = 4.6$ for vortex shedding suppression.
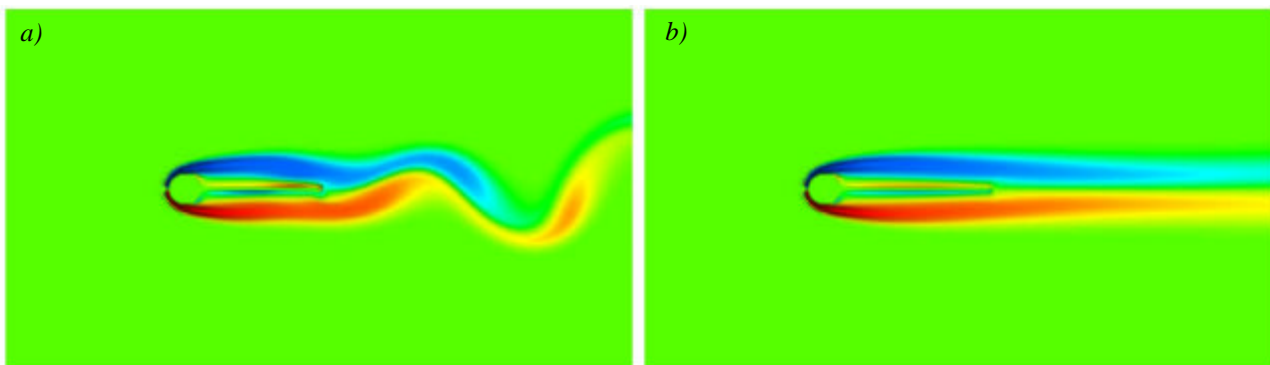

Figure 9. Vorticity fields for $Re = 160$ at time $t \cdot U_\infty/D = 248$; a) l/D = 4 and b) l/D = 5.

4.2. Two-dimensional simulation of three-dimensional flows

It is truth that for Reynolds numbers higher than 170 that the three-dimensionality has a major role, which could suggest that two-dimensional simulations are not able to represent its features. But in terms of shedding frequency this is not the truth at all once one gets to the Reynolds numbers higher than 250. In these cases the Strouhal numbers resulting are slightly affected by the three-dimensionality, in such a way that two-dimensional simulations achieve similar shedding frequencies, as one can see comparing the experimental data against the 2D simulations on Fig. (5). This way it was found worth to analyze two-dimensionally this flow patterns, always concerning that one might be very careful to jump into conclusions after these two-dimensional simulations results.

Simulations at $Re = 300$ for cylinders with attached splitter plates were performed for plate lengths, l/D, equal to 2 ($S = 0.203$), 4 ($S = 0.123$), 6 ($S = 0.086$) and 8 ($S = 0.063$). The results obtained by the present simulations are plotted together with other results showing an interesting phenomena on Strouhal Number as one increases the plate length (Fig. 10).
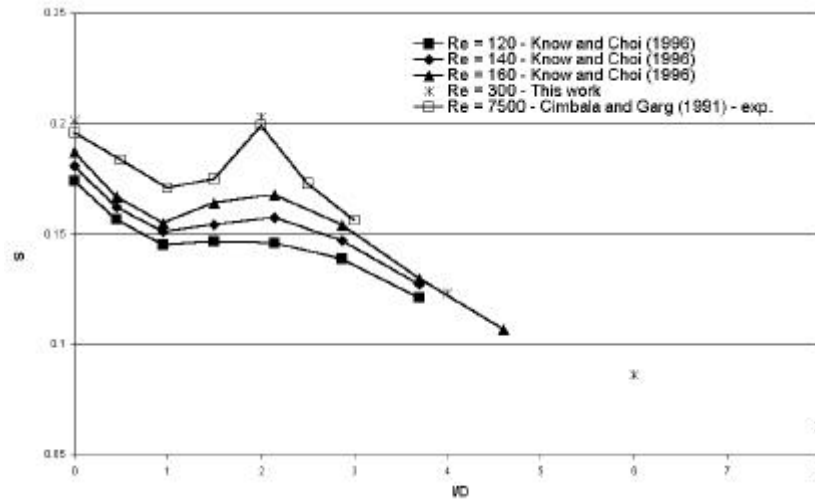

Figure 10. Strouhal number vs. plate length behind circular cylinder for different Re.

There is a notable increasing on the Strouhal number for the plate lengths $1 < l/D < 2$. Bearman (1965) suggests that this phenomena is associated to a critical length where the plate induces the vortices to break down from the shear layers upstream to the end of the plate, developing not fully formed vortices. The present results for $Re = 300$ showed to be unable to correctly represent this phenomena due to the small number of simulations performed until this moment, but partial results show a increase of 1% on the Strouhal number for $l/D = 2$, and an extraordinary decrease for further lengths.

In the $Re = 160$ simulations appears an interesting vortex at the edge of the plate. This structure had already been recognized by Know and Choi (1996) but no further study about it's formation and influence on the flow have been found. In this work this eddy formation could be found also at higher Reynolds numbers, where it looks stronger and better defined.

Due to the presence of the plate, the shear layer that starts on the surface of the cylinder generates vorticity of opposite signal over the plate, as one can see following vortices B and B' in Fig. (11a).
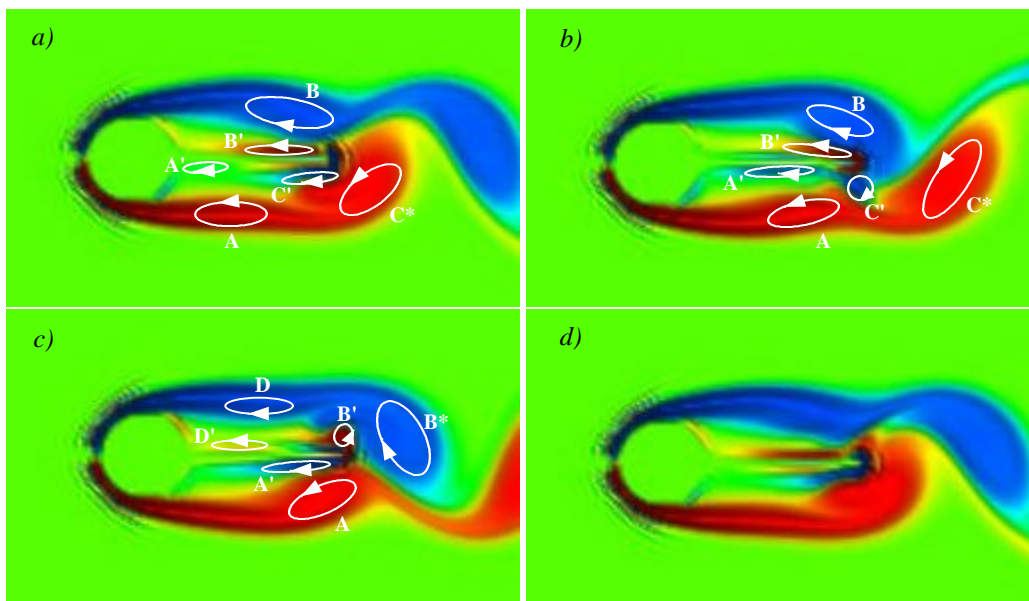

Figure 11. Vorticity field for $Re = 300$ and $l/D = 2$. $Dt \cdot U_\infty/D$ between each image equal to 1,49.

Vortex B' moves together with vortex B along the plate, while at this same moment vortex C' is ahead of vortex B' and gets trapped at the end of the plate by vortex C*. At Fig. (11*b*) vortex B' gets trapped on the plate's edge while vortex C' is paring with vortex B.

At Fig. (11*c*) vortex B* is the result of the paring between vortices C' and B, and it traps the growing vortex B' that can be seen paring with vortex A at Fig. (11*d*), where there is again nearly the same vorticity field as in the first image.

In order to study how this vortex frequency influence the wake, the velocity signals and their respective frequency spectrums have been analyzed at several positions over the domain, as shown in Fig. (12).
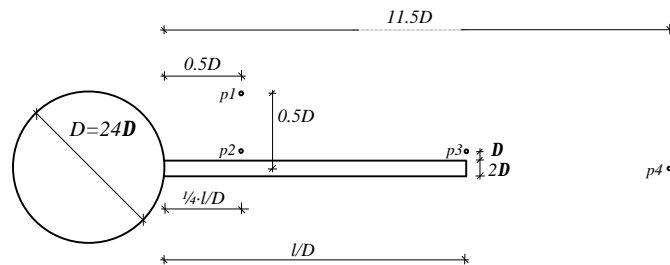

Figure 12. Location of probes near the obstacle.

The probe *p1* has been placed to achieve the breaking shear layer's signal, while probes *p2* and *p3* are placed to get the velocity signals near the plate's surface respectively before and at the plate's edge, finally probe *p4* has been placed to get the frequency spectrum at the wake.

As one can see in Fig. (13) the power spectrum density on the wake for *Re* = 300 ($x/D = 1$, $y/D = 0$), on a situation with no plate has well defined peaks which are stronger on the odd multiples of the main frequency.
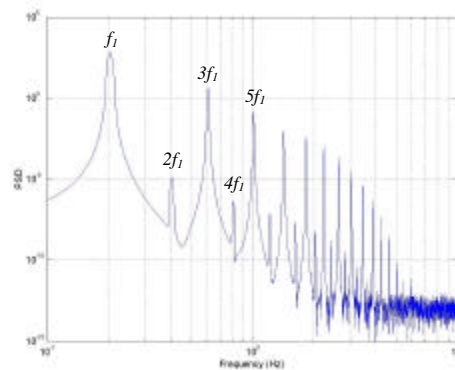

Figure 13. Power Spectrum Density at Re = 300 for a circular cylinder with no splitter plate, $x/D = 1$, $y/D = 0$.

This spectrum behavior changes slightly with the plate's presence at the *p1* location as seen at Fig. (14*a*). Here the signal is expected to be barely affected by the presence of the plate. In fact one can take note of the absence of higher frequencies and that there is not much difference between odd and even multiples.

The same behavior is verified at *p2* (but the signal has less energy), Fig. (14*b*), suggesting that at these locations there is a direct interaction between the shear layer and the boundary-layer over the plate.

One can see at *p3* frequency spectrum, Fig. (14*c*), the clear presence of higher frequencies, not strong on the previous signals, suggesting that this new frequencies are associated with the growth of the eddy at the plate's edge.

At *p4* location one finds a frequency spectrum very similar to the one of the flow without plate, Fig. (14*d*). But in comparison with *p1*, *p2* and *p3* spectra one can clearly notice less energy on the odd multiple of the main frequency.

5. Conclusions

The virtual boundary method used together with a uniform cartesian mesh, in comparison to the solution of the Navier-Stokes equations over a body-fitted mesh with curvilinear coordinates, permits the use of a small computational demand obtaining satisfactory results.

The use of splitter plates to control bluff-bodies' vortex shedding shows to be of great efficiency. As it has been shown, attached plates perform great changes on the shedding frequency depending on the length.

At first, the end plate vortex seemed to have a major role on the shedding frequency, but further studies showed that it has no influence on the major frequency, and its shedding is governed by the Kármán vortex trail and by the recirculation region behind the obstacle.
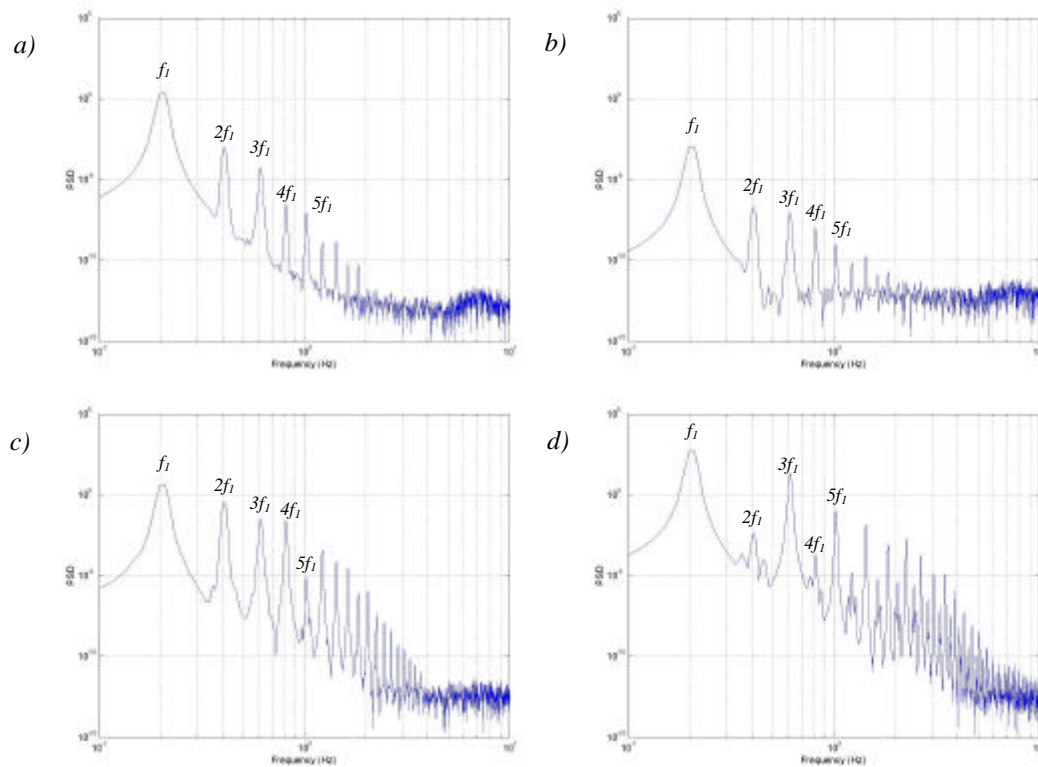
Figure 14. Power Spectrum Density for *Re* = 300 and *l/D* = 2. *a) p1, b) p2, c) p3* and *d) p4*.

6. Acknowledgement

7. References

Arie, M. and Rouse, H., 1956, "Experiments on two-dimensional flow over a normal wall", Journal of Fluid Mechanics, Vol. 1, Part 2.

Bearman, P. W., 1965, "Investigation of the flow behind a two-dimensional model with blunt trailing edge and fitted with splitter plates", Journal Fluid Mechanics, Vol. 21, part 2, p. 241-255.

Berger, E. and Wille, R., 1972, "Periodic flow phenomena", Ann. Rev. Fluid. Mech., Vol. 4, p. 313-340.

Cimbala, J. M. and Garg, S., 1991, "Flow in the wake of a freely rotatable cylinder with splitter plate", AIAA Journal, Vol. 29, p. 1001-1006.

Goldstein, D., Handler, R. and Sirovich, L., 1993, "Modeling a no-slip flow boundary with an external force field", Journal of Computational Physics, Vol. 105, p. 345-366.

Know, K. and Choi, H., 1996, "Control of laminar vortex shedding behind a circular cylinder using splitter plates", Physics of Fluids, Vol. 8, No. 2, p. 479-486.

Lamballais, E. and Silvestrini, J., 2002, "Direct numerical simulation of interactions between and mixing layer and a wake around a cylinder", (in press) J. of Turbulence.

Lele, S. K., 1992, "Compact finite difference schemes with spectral-like resolution", Journal of Computational Physics, Vol. 103, p.16-42.

Pérsillon, H. and Braza, M., 1998, "Physical analysis of the transition to turbulence in the wake of a circular cylinder by three-dimensional Navier-Stokes simulation", Journal of Fluid Mechanics, Vol. 365, p. 23-88.

Roshko, A., 1954, "On the drag and the shedding frequency of two-dimensional bluff bodies", NACA TN 3169, 29 p.

Roshko, A., 1993, "Perspectives on bluff body aerodynamics", Journal of Wind Engineering and Industrial Aerodynamics, Vol. 49, p. 79-100.

Saiki, E. M. and Biringen, S. 1996, "Numerical simulation of a cylinder in uniform flow: application of a virtual boundary method", Journal of Computational Physics, Vol. 123, p.450-465.

Schumm, M., Berger, E. and Monkewitz, P. A., 1994, "Self-excited oscillations in the wake of two-dimensional bluff bodies and their control", Journal of Fluid Mechanics, Vol. 271, pp.17-53.

Silvestrini, J. and Lamballais, E., 2002, "Direct numerical simulation of wakes using virtual cylinders", (in press) Int. J. of Computational Fluids Dynamics.

Williamson, J. H., 1980, "Low-storage Runge-Kutta schemes", Journal of Computational Physics, Vol. 35, p. 48-56.

Williamson, C. H. K., 1989, "Oblique and parallel modes of vortex shedding in the wake of a circular cylinder at low Reynolds numbers", Journal of Fluid Mechanics, Vol. 206, pp. 579-627.

Williamson, C. H. K., 1996, "Three-dimensional wake transition", Journal of Fluid Mechanics, Vol. 328, pp. 345-407.